

LA-UR-16-23696 (Accepted Manuscript)

Purcell effect at the percolation transition

Szilard, Daniela
de Melo Kort-Kamp, Wilton Junior
Rosa, Felipe
Pinheiro, Felipe
Farina, Carlos

Provided by the author(s) and the Los Alamos National Laboratory (2017-01-12).

To be published in: Physical Review B

DOI to publisher's version: 10.1103/PhysRevB.94.134204

Permalink to record: <http://permalink.lanl.gov/object/view?what=info:lanl-repo/lareport/LA-UR-16-23696>

Disclaimer:

Approved for public release. Los Alamos National Laboratory, an affirmative action/equal opportunity employer, is operated by the Los Alamos National Security, LLC for the National Nuclear Security Administration of the U.S. Department of Energy under contract DE-AC52-06NA25396. Los Alamos National Laboratory strongly supports academic freedom and a researcher's right to publish; as an institution, however, the Laboratory does not endorse the viewpoint of a publication or guarantee its technical correctness.

Purcell effect at the percolation transition

D. Szilard,¹ W. J. M. Kort-Kamp,² F. S. S. Rosa,¹ F. A. Pinheiro,¹ and C. Farina¹

¹*Instituto de Física, Universidade Federal do Rio de Janeiro,
Caixa Postal 68528, Rio de Janeiro 21941-972, RJ, Brazil*

²*Theoretical Division and Center for Nonlinear Studies, MS B258,
Los Alamos National Laboratory, Los Alamos, New Mexico 87545, United States*

(Dated: July 26, 2016)

We investigate the spontaneous emission rate of a two-level quantum emitter next to a composite medium made of randomly distributed metallic inclusions embedded in a dielectric host matrix. In the near-field, the Purcell factor can be enhanced by two-orders of magnitude relative to the case of an homogenous metallic medium, and reaches its maximum precisely at the insulator-metal transition. By unveiling the role of the decay pathways on the emitter's lifetime, we demonstrate that, close to the percolation threshold, the radiation emission process is dictated by electromagnetic absorption in the heterogeneous medium. We show that our findings are robust against change in material properties, shape of inclusions, and apply for different effective medium theories as well as for a wide range of transition frequencies.

I. INTRODUCTION

In cavity quantum electrodynamics, spontaneous emission (SE) is a pivotal example of energy transfer from an excited quantum emitter (atom, molecule, or quantum dot) into its environment. As first predicted by Purcell [1] and later experimentally confirmed by Drexhage *et al.* [2], the environment exerts a crucial influence on the emitters' decay. Indeed, the presence of objects in the system allow for new energy relaxation channels (*e. g.* plasmonic excitations) that can strongly affect the emitter's lifetime [3]. The influence of the environment on the emitter's SE rate characterizes the Purcell effect and is quantified by the local density of states (LDOS). Typically, a modification of the LDOS involves either changing the environment geometry or its material properties [4].

The last decade has witnessed an increasing research effort towards the control of SE rate due to the notable progresses in near-field optics, plasmonics, and metamaterials. Advances in nano-optics have not only allowed the improvement of the spectroscopical resolution of molecules in complex environments [5], but have also led to the use of nanometric objects (*e.g.* nanoparticles and nanotips) that modify the lifetime and enhance the fluorescence of single molecules [6, 7]. The advent of plasmonic devices and metamaterials has also opened new possibilities for tailoring the SE rate. Indeed, the local field enhancement due to excitation of plasmonic resonances has been explored in several applications, such as the surface-enhanced Raman scattering [8–10], and the modification of two-level atom resonance fluorescence [11]. In addition, photonic crystals [12], optical cavities [13], metallic nanostructures [14, 15], plasmonic cloaks [16, 17], hyperbolic metamaterials [18], ENZ metamaterials [19–22] and negative index materials [23] are some examples of systems in which the LDOS and SE rate are dramatically affected by unusual photonic properties of the environment. Besides, gated and magnetic field biased graphene correspond to systems where active control of the Purcell effect can be implemented [24, 25]. However, in most of previous examples the modification of the LDOS involves sophisticated nano-fabrication techniques and/or complex nanostructures.

In the present paper, we propose an alternative material platform, of easy fabrication, to tailor and control the SE of quantum emitters, namely, composite media. Our study is motivated by recent experimental observations that the SE is modified in the presence of metallic, semicontinuous media [26–28]. Specifically, we have investigated the SE rate of a two-level atom in the vicinities of a semi-infinite medium composed of metallic inclusions, with various shapes and concentrations, embedded in a dielectric host medium. Applying different homogenization techniques (Bruggeman [29] and Lagarkov-Sarychev [30]), we demonstrate that the SE rate is remarkably enhanced in composite media in relation to the case where homogeneous media are considered. In particular, we show that SE rate is maximal precisely at the insulator-metal transition (percolation threshold). We demonstrate that these results are independent of the shape and material of the inclusions, and are valid for a broad range emission wavelengths. Altogether our findings suggest that composite media could be exploited in the design of novel, versatile materials in applications involving the radiative properties of light emitters.

The paper is organized as follows. In Sec. II we present the employed methodology and the effective medium theory used to model the effective electric permittivity of the composite medium. In Sec. III we present our main results and the related discussions, while in Sec. IV we summarize the results and conclude.

II. METHODOLOGY

A. The Purcell Effect

Let us consider a two-level emitter at a distance z of a semi-infinite medium composed of randomly distributed metallic inclusions (electric permittivity ϵ_i) embedded in a dielectric host matrix (electric permittivity ϵ_{hm}), as shown in Fig. 1. In the presence of an arbitrary environment, the SE rate of a two-level atom at position \mathbf{r} reads [3]

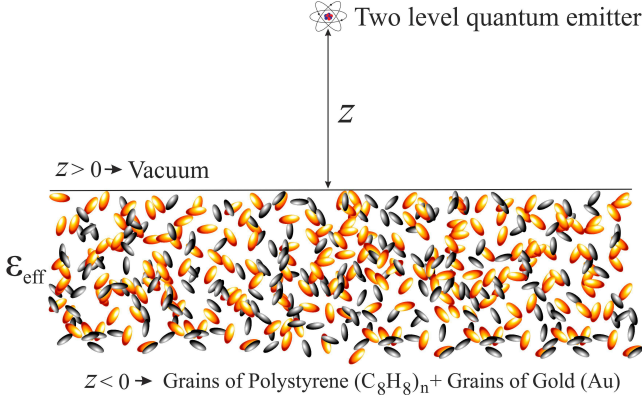


Figure 1. Schematic view of the system under investigation: a two-level emitter at a distance z of a half-space composed of metallic (gold) inclusions embedded in a dielectric (polystyrene) host matrix.

$$\Gamma_{21} = \frac{6\pi c}{\omega_0} \Gamma^{(0)} \text{Im}\{\mathbf{n} \cdot \mathbb{G}(\mathbf{r}, \mathbf{r}; \omega_0) \cdot \mathbf{n}\}, \quad (1)$$

where $\Gamma^{(0)} = \omega_0^3 |\mathbf{d}_{21}|^2 / 3\pi\hbar\epsilon_0 c^3$ is the free-space SE rate, $\omega_0 = k_0 c$ is the transition frequency, \mathbf{d}_{21} the emitter's transition electric dipole moment, $\mathbf{n} = \mathbf{d}_{21} / |\mathbf{d}_{21}|$, and $\mathbb{G}(\mathbf{r}, \mathbf{r}'; \omega)$ is the dyadic Green function of the system. The influence of the surrounding bodies on the emitter's lifetime is coded into $\mathbb{G}(\mathbf{r}, \mathbf{r}'; \omega)$, which satisfies

$$\nabla \times \nabla \times \mathbb{G}(\mathbf{r}, \mathbf{r}'; \omega) - \frac{\omega^2}{c^2} \mathbb{G}(\mathbf{r}, \mathbf{r}'; \omega) = \mathbb{I} \delta(\mathbf{r} - \mathbf{r}'). \quad (2)$$

In free-space the dyadic Green function can be cast as (for $z > z'$)

$$\mathbb{G}^{(0)}(\mathbf{r}, \mathbf{r}'; \omega) = \frac{i}{2} \int \frac{\mathbb{M} e^{i\mathbf{k}_{\parallel} \cdot (\mathbf{r} - \mathbf{r}') + k_{z0}(z - z')}}{k_{z0}} \frac{d^2 \mathbf{k}_{\parallel}}{(2\pi)^2}, \quad (3)$$

where $k_{z0} = \sqrt{k_0^2 - k_{\parallel}^2}$ and \mathbb{M} is given by

$$\mathbb{M} = \epsilon_{\text{TE}}^+ \otimes \epsilon_{\text{TE}}^+ + \epsilon_{\text{TM}}^+ \otimes \epsilon_{\text{TM}}^+, \quad (4)$$

with the TE- and TM-polarization vectors defined as

$$\epsilon_{\text{TE}}^{\pm} = \frac{-k_y \hat{\mathbf{x}} + k_x \hat{\mathbf{y}}}{k_{\parallel}}, \quad \text{and} \quad \epsilon_{\text{TM}}^{\pm} = \frac{\pm k_{z0} \mathbf{k}_{\parallel} - k_{\parallel}^2 \hat{\mathbf{z}}}{k_{\parallel} k_0}. \quad (5)$$

Note that these vectors are orthogonal, but they are normalized only for propagating modes ($k_{\parallel} < k_0$). Substituting Eq. (3) into (1) and using that at the coincidence the only non vanishing components of $\mathbb{G}^{(0)}$ are $\mathbb{G}_{xx}^{(0)} = \mathbb{G}_{yy}^{(0)}$ and $\mathbb{G}_{zz}^{(0)}$ one can show that $\Gamma_{21} = \Gamma^{(0)}$, as it should be.

In an inhomogeneous environment Eq. (3) does not give the full Green function of the problem. In this case the dyadic Green function has to be modified in order to satisfy the electromagnetic field boundary conditions and to take into account scattering owing to neighboring objects. Particularly,

for an emitter close to a half-space presenting a flat interface at $z = 0$, one can write $\mathbb{G}(\mathbf{r}, \mathbf{r}'; \omega) = \mathbb{G}^{(0)}(\mathbf{r}, \mathbf{r}'; \omega) + \mathbb{G}^{(S)}(\mathbf{r}, \mathbf{r}'; \omega)$, where [3]

$$\mathbb{G}^{(S)}(\mathbf{r}, \mathbf{r}'; \omega) = \frac{i}{2} \int \frac{\mathbb{R} e^{i\mathbf{k}_{\parallel} \cdot (\mathbf{r} - \mathbf{r}') e^{ik_{z0}(z+z')}}}{k_{z0}} \frac{d^2 \mathbf{k}_{\parallel}}{(2\pi)^2}, \quad (6)$$

is the Green function associated to the electromagnetic field generated by the oscillating dipole source and scattered (reflected) by the semi-infinite medium. \mathbb{R} is the half-space reflection matrix given by

$$\mathbb{R} = \sum_{i, j = \{\text{TE}, \text{TM}\}} r^{i,j} \epsilon_i^+ \otimes \epsilon_j^-, \quad (7)$$

where $r^{i,j}$ ($i, j = \text{TE}, \text{TM}$) corresponds to the reflection coefficient for incoming j -polarized light that is reflected as an i -polarized wave.

Given this system geometry, one can decompose the SE rate in two contributions $\Gamma_{21} = \Gamma_{\perp} + \Gamma_{\parallel}$. Here, Γ_{\perp} (Γ_{\parallel}) expresses the decay rate contribution due to the transition dipole moment component perpendicular (parallel) to the vacuum-medium interface. Plugging Eqs. (3)-(7) into Eq. (1) one can show that [25]

$$\frac{\Gamma_{\perp}}{\Gamma^{(0)}} = \frac{d_z^2}{|\mathbf{d}_{21}|^2} \left\{ 1 + \frac{3}{2} \int_0^{k_0} \frac{k_{\parallel}^3}{k_0^3 \xi} \text{Re} [r^{\text{TM}, \text{TM}} e^{2i\xi z}] dk_{\parallel} + \frac{3}{2} \int_{k_0}^{\infty} \frac{k_{\parallel}^3}{k_0^3 \zeta} e^{-2\zeta z} \text{Im} [r^{\text{TM}, \text{TM}}] dk_{\parallel} \right\}, \quad (8)$$

and

$$\frac{\Gamma_{\parallel}}{\Gamma^{(0)}} = \frac{d_{\parallel}^2}{|\mathbf{d}_{21}|^2} \left\{ 1 + \frac{3}{4} \int_0^{k_0} \frac{k_{\parallel}}{k_0^3 \xi} \text{Re} [(k_0^2 r^{\text{TE}, \text{TE}} - \xi^2 r^{\text{TM}, \text{TM}}) e^{2i\xi z}] dk_{\parallel} + \frac{3}{4} \int_{k_0}^{\infty} \frac{k_{\parallel}}{k_0^3 \zeta} \text{Im} [k_0^2 r^{\text{TE}, \text{TE}} + \zeta^2 r^{\text{TM}, \text{TM}}] e^{-2\zeta z} dk_{\parallel} \right\}, \quad (9)$$

where $\xi = \sqrt{k_0^2 - k_{\parallel}^2}$ and $\zeta = \sqrt{k_{\parallel}^2 - k_0^2}$. In the cases we consider $r^{\text{TE}, \text{TE}}$ and $r^{\text{TM}, \text{TM}}$ will be given by the usual Fresnel reflection coefficients for a flat interface between vacuum and an homogeneous medium, namely [3]

$$r^{\text{TE}, \text{TE}} = \frac{k_{z0} - k_{z1}}{k_{z0} + k_{z1}}, \quad r^{\text{TM}, \text{TM}} = \frac{\epsilon_e k_{z0} - k_{z1}}{\epsilon_e k_{z0} + k_{z1}}, \quad (10)$$

where ϵ_e is the effective dielectric constant of the substrate (see next section) and $k_{z1} = \sqrt{\epsilon_e k_0^2 - k_{\parallel}^2}$. Finally, note that for an isotropic atom we have $d_z^2 / |\mathbf{d}_{12}|^2 = 1/3$ and $d_{\parallel}^2 / |\mathbf{d}_{12}|^2 = 2/3$.

B. Effective Medium Theory

Effective medium theories allow one to construct an effective dielectric constant ϵ_e of a composite medium as a function

of its constituents' properties (dielectric constants and shapes) as well as of the fractional volumes characterizing the mixture [29–32].

One of the most important and successful effective medium approaches is the Bruggeman Effective Medium Theory (BEMT), which is the simplest analytical model that predicts an insulator-metal transition at a critical concentration of metallic particles in the dielectric host [29, 33]. BEMT treats the dielectric host medium and the metallic inclusions symmetrically, and it is based on the following assumptions: (i) the grains are randomly oriented spheroidal particles, and (ii) they are embedded in an homogeneous effective medium of dielectric constant ε_e that will be determined self-consistently [33]. In this work we consider spheroidal inclusions whose geometry is characterized by the depolarization factor $0 \leq L \leq 1$. Explicit expressions of L in terms of the eccentricity e of the spheroid are [34]

$$L = \begin{cases} \frac{1 - e^2}{2e^3} \left[\ln \left(\frac{1 + e}{1 - e} \right) - 2e \right], & \text{prolate spheroid} \\ \frac{1 + e^2}{e^3} [e - \arctan(e)], & \text{oblate spheroid} \end{cases} \quad (11)$$

Within the BEMT ε_e is computed by demanding that the average over all directions of the scattered Poynting vector vanish when the system is illuminated by a monochromatic wave with wavelength (both in vacuum and inside the medium) much larger than the size of the inclusions. In this case, the effective permittivity satisfies the following equation [29–32, 34],

$$(1 - f) \left\{ \frac{\varepsilon_{hm} - \varepsilon_e}{\varepsilon_e + L(\varepsilon_{hm} - \varepsilon_e)} + \frac{4(\varepsilon_{hm} - \varepsilon_e)}{2\varepsilon_e + (1 - L)(\varepsilon_{hm} - \varepsilon_e)} \right\} + f \left\{ \frac{\varepsilon_i - \varepsilon_e}{\varepsilon_e + L(\varepsilon_i - \varepsilon_e)} + \frac{4(\varepsilon_i - \varepsilon_e)}{2\varepsilon_e + (1 - L)(\varepsilon_i - \varepsilon_e)} \right\} = 0, \quad (12)$$

where ε_i , ε_{hm} are the dielectric constants of the metallic inclusions and host matrix, respectively, and f ($0 \leq f \leq 1$) is the volume filling factor for the metallic inclusions. Equation (12) has several roots but only the one with $\text{Im}(\varepsilon_e) \geq 0$ is physical since we are assuming passive materials (*i. e.*, no optical gain).

The percolation threshold f_c corresponds to a critical value of the filling factor for which the composite medium undergoes an insulator-conductor transition, thereby exhibiting a dramatic change in its electrical and optical properties [30–35]. This critical filling factor is calculated by taking the quasi-static limit ($\omega \rightarrow 0$) in Eq. (12). In this limit, $\varepsilon_i \gg \varepsilon_{hm}$, $\text{Im}[\varepsilon_i] \gg \text{Re}[\varepsilon_i]$, and $\text{Im}[\varepsilon_{hm}] \ll \text{Re}[\varepsilon_{hm}]$ provided the host medium does not have a resonance near $\omega = 0$. Consequently, ε_i (ε_{hm}) may be approximated by a pure imaginary (real) function. Besides, if $f < f_c$ ($f \geq f_c$) the effective medium behaves as a dielectric-like (metal-like) material so that $\text{Re}[\varepsilon_e] > 0$ ($\text{Re}[\varepsilon_e] < 0$) in the low frequency regime. Hence, the critical threshold filling factor can be obtained by the condition $\text{Re}[\varepsilon_e] = 0$. For spheroidal inclusions the BEMT predicts that the percolation transition occurs at [30–

32, 34]

$$f_c^B(L) = \frac{L(5 - 3L)}{(1 + 9L)}. \quad (13)$$

In order to test the robustness of our results with respect to specific features of a given effective medium theory, we shall consider an alternative homogenization technique proposed by Lagarkov and Sarychev in Ref. [30] as well. The Lagarkov-Sarychev approach is known to give more accurate results for f_c than the BEMT in the regime of small L ($L \ll 1$); the critical filling factor within the Lagarkov-Sarychev effective medium theory is [30]

$$f_c^{LS}(L) = \frac{9L(1 - L)}{2 + 15L - 9L^2}. \quad (14)$$

In the following section the SE rate of an emitter close to a semi-infinite composite medium will be computed by means of the effective medium approaches described above. The dielectric functions of the metallic inclusions ε_i and of the dielectric host-medium ε_{hm} are

$$\varepsilon_i(\omega) = 1 - \frac{\omega_{pi}^2}{\omega^2 + i\gamma_i\omega}, \quad (15)$$

$$\varepsilon_{hm}(\omega) = 1 + \sum_j \frac{\omega_{pj}^{hm2}}{\omega_{Rj}^2 - \omega^2 - i\omega\Gamma_j}, \quad (16)$$

where ω_{pi} (ω_{pj}^{hm}) and γ_i (Γ_j) are, respectively, the plasma frequency (oscillating strengths) and the inverse of the relaxation time(s) of the metallic inclusions (host medium). The value of these parameters for the metals (Au, Cu, Ti, Ag) and dielectrics (polystyrene) considered were extracted from Refs. [36–38].

III. RESULTS AND DISCUSSIONS

In Fig. 2 the SE rate is calculated as a function of the distance between the emitter and the semi-infinite medium made of spherical ($L = 1/3$) gold inclusions embedded in a polystyrene host matrix for different values of the filling fractions f . Within BEMT the dielectric constant of the composite medium presents a dielectric-like (metal-like) response for $f < 1/3$ ($f > 1/3$) [33]. The emitter is assumed to be a Caesium (Cs) atom with transition wavelength $\lambda = 450 \mu\text{m}$, that is, in the THz frequency range. It is clear that the composite media may greatly enhance the SE rate when compared to the homogeneous cases $f = 0$ and $f = 1$ for both transition electric dipole parallel and perpendicular to the flat interface. Indeed, in the presence of the composite media the emitter's decay rate may be five to six orders of magnitude times larger than its value in free space for distances $z \sim 100 \text{ nm}$, as it can be seen in Figs. 2a and 2b for Γ_{\parallel} and Γ_{\perp} , respectively. Figure 2 also reveals that the transition from far- to near-field effects on the emitter's lifetime can be tuned by the filling factor f . Interestingly, for $f = f_c^B = 1/3$ near-field effects become relevant even for distances of the order of $z \sim 1 \mu\text{m}$.

Similar qualitative results hold for the perpendicular configuration, even though f seems to play a less prominent role in the near-to-far-field transition distance range.

It should be noticed that in the far-field regime the dependence of the SE rate on f is very weak, where the expected oscillatory behavior occurs for $z \gtrsim 10 \mu\text{m}$. For large distances Γ_{\parallel} and Γ_{\perp} can be approximated by the first integrals in Eqs. (8) and (9) with the main contribution originating from electromagnetic modes with $k_{z0} = \xi \simeq 0$ (due to the oscillatory behavior of $e^{2i\xi z}$). An expansion of the reflection coefficients around $k_{z0} = 0$ shows that $r^{\text{TE, TE}} \simeq r^{\text{TM, TM}} \simeq -1 + \mathcal{O}(\xi/k_0)$ and, hence, the dominant contribution to the emitter's decay rate in the far-field does not carry information about the electromagnetic properties of the substrate. On the other hand, the metal concentration strongly affects the Purcell effect for distances $z \lesssim 1 \mu\text{m}$. For such distances light emission is more affected by electromagnetic evanescent modes ($k_{\parallel} > k_0$) that exist only close to the air-substrate interface. Particularly, in the extreme near-field regime an approximate analytic expression for the SE rate can be obtained by taking the quasi-static limit ($c \rightarrow \infty$) in Eqs. (8) and (9),

$$\frac{\Gamma_{\perp}}{\Gamma^{(0)}} \simeq 2 \frac{\Gamma_{\parallel}}{\Gamma^{(0)}} \simeq \frac{3}{8} \frac{1}{k_0^3 z^3} \frac{\text{Im}[\varepsilon_e]}{|\varepsilon_e + 1|^2}. \quad (17)$$

Note that the z^{-3} distance scaling-law for bulk materials is rederived regardless of the optical characteristics of the substrate. On the one hand, for low values of f the decay rate dynamics is governed by the (small) losses in the dielectric host since $\Gamma_{\perp, \parallel}$ are proportional to $\text{Im}[\varepsilon_e] \simeq \text{Im}[\varepsilon_{hm}] \ll 1$. The SE rate increases as small amounts of metallic inclusions are added to the host matrix due to enhancement of absorption processes in the substrate. On the other hand, large concentrations of metal lead to SE rates proportional to $1/\text{Im}[\varepsilon_e] \simeq 1/\text{Im}[\varepsilon_i] \ll 1$. Based on this analysis, it's clear that the emitter's lifetime will be greatly modified by f , as seen in Figs. 2a and b for $z \lesssim 1 \mu\text{m}$.

The fact that in the near-field regime $\Gamma_{\perp, \parallel}$ initially grows with $\text{Im}[\varepsilon_e]$ ($f \ll 1$) and then decays with $1/\text{Im}[\varepsilon_e]$ ($f \simeq 1$) suggests that the decay rate should present a peak at some critical filling factor. Remarkably, the SE rate reaches its maximum value at $f_c^B = 1/3$ (see Fig. 3), which precisely corresponds to the percolation transition threshold predicted by the BEMT for spherical inclusions. At f_c^B the value of the SE can be more than two orders of magnitude larger than its values for other inclusions' concentrations ($f \neq f_c^B$) and for distances $z \lesssim 1 \mu\text{m}$. In the insets of Fig. 2, the relative variation of the SE rate with respect to its value in the presence of an homogeneous gold semi-infinite medium ($f = 1$),

$$\frac{\Delta\Gamma_{\perp, \parallel}}{\Gamma_{\perp, \parallel}(f=1)} \equiv \frac{\Gamma_{\perp, \parallel} - \Gamma_{\perp, \parallel}(f=1)}{\Gamma_{\perp, \parallel}(f=1)}, \quad (18)$$

is calculated as a function of z . In both parallel and perpendicular cases, $\Delta\Gamma_{\perp, \parallel}/\Gamma_{\perp, \parallel}(f=1)$ is largely enhanced at the percolation transition f_c^B , specially for shorter distances $z \lesssim 1 \mu\text{m}$. This relative variation can be as impressive as 500

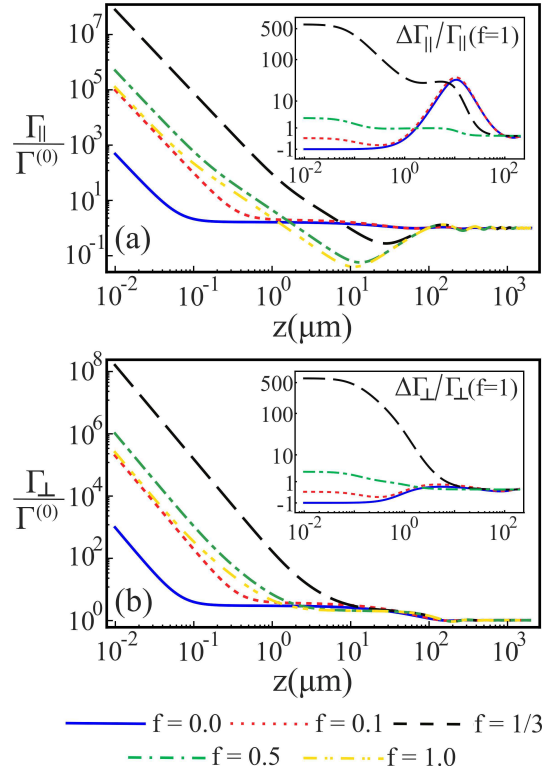


Figure 2. Spontaneous emission rate dependence with the distance z to the semi-infinite composite medium (BEMT) for parallel (a) and perpendicular (b) transition dipole orientations. In both panels the metallic inclusions are made of gold and $L = 1/3$ (spheres). The insets display the SE rates relative to the $f = 1$ case, i. e., when the emitter is in presence of an homogeneous gold substrate, for the same values of f as before.

at f_c^B , unambiguously demonstrating that composite media can largely outperform homogeneous media, when it comes to modify and tune the SE rate.

In order to further investigate the dependence of the SE rate on the filling fraction f , in Fig. 3 the behavior of Γ_{\perp} and Γ_{\parallel} as a function of f is depicted for different distances z between the emitter and the composite medium. Figure 3 shows that for distances $z \lesssim 1 \mu\text{m}$ the decay rate reaches its maximal value exactly at the percolation threshold f_c^B , in both parallel and perpendicular configurations. For distances smaller than $1 \mu\text{m}$ the results of Fig. 3 are well described by Eq. (17). As a consequence, in this regime the enhancement in the Purcell effect at f_c^B relative to the homogeneous gold semi-infinite medium is distance-independent,

$$\frac{\Gamma_{\perp, \parallel}(f = f_c^B)}{\Gamma_{\perp, \parallel}(f = 1)} \simeq \frac{\text{Im}[\varepsilon_e] |\varepsilon_i + 1|^2}{\text{Im}[\varepsilon_i] |\varepsilon_e + 1|^2}. \quad (19)$$

For other distances $z \lesssim 10 \mu\text{m}$ the enhancement at f_c^B is of one order of magnitude or less. Figure 3 also emphasizes the importance of near-field effects, as the SE rate enhancement becomes small for distances $z \gtrsim 10 \mu\text{m}$ and completely disappears at $z \sim 1 \text{mm}$.

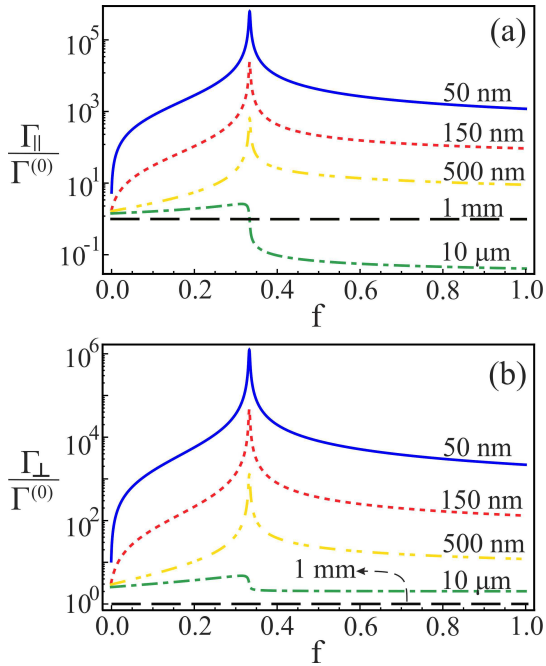


Figure 3. Spontaneous emission rate as a function of the volume filling factor f for parallel $\Gamma_{\parallel}/\Gamma^{(0)}$ (a) and perpendicular $\Gamma_{\perp}/\Gamma^{(0)}$ (b) cases. Results were computed for several z -distances between the emitter and the semi-infinite medium. All other parameters are the same as in Fig. 2. Both panels reveal that maximum enhancement in the SE rate occurs at the insulator metal transition $f_c^B = 1/3$.

It is interesting to comment that a large enhancement of heat transfer between composite bodies at the percolation threshold also occurs due to near-field effects [34]. Here the role of the near-field is similar and it helps one to qualitatively understand the physical origin of the SE rate enhancement at f_c . Indeed, the physical explanation of these two distinct phenomena (SE decay rate and near heat field transfer) in the presence of composite media are intrinsically related to the universal properties of the percolation phase transition, in particular the enhanced and scale invariant current and electric field fluctuations that take place close to the percolation critical point [35]. These enhanced electric field fluctuations modify the structure of the electromagnetic modes, and hence show up in the LDOS. For composite media around the percolation threshold, extremely localized and subwavelength confined resonant plasmon excitations occur, leading to the formation of giant spatial fluctuations of the electromagnetic field intensity (“hot spots”) [35]. As the existence of localized modes has been demonstrated to strongly amplify the LDOS [26], we conclude that the SE rate should be enhanced at the insulator-metal transition as well. These arguments qualitatively explain the results reported in Figs. 2 and 3.

The influence of the various possible inclusions shapes in the SE rate is shown in Fig. 4, where Γ_{\parallel} is calculated as a function of both the filling fraction f and the depolarization factor L for $z = 50$ nm [(a) and (c)] and $z = 500$ nm [(b) and (d)]. In panels (a) and (b) the effective dielectric constant of the substrate was obtained using BEMT whereas (c) and (d)

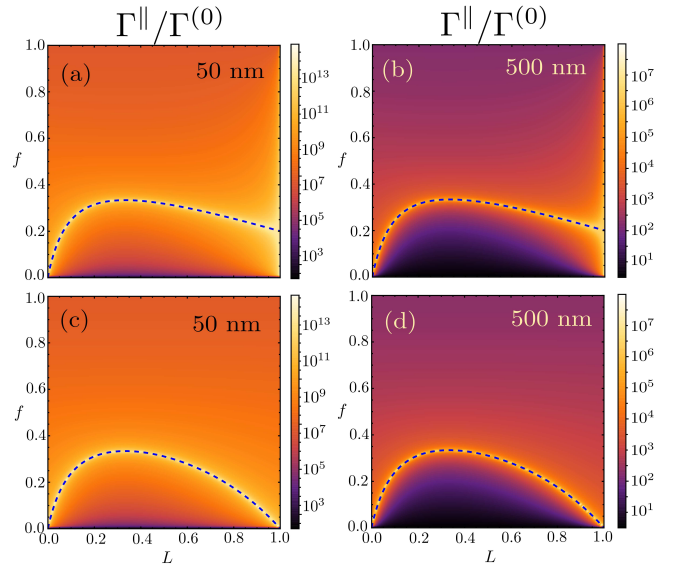


Figure 4. Density plots of $\Gamma_{\parallel}/\Gamma^{(0)}$ as a function of both filling factor f and the depolarization factor L for $z = 50$ nm (a) and (c), and $z = 500$ nm (b) and (d). Panels (a) and (b) correspond to calculations using the Bruggeman effective medium theory whereas (c) and (d) to the Lagarkov-Sarychev approach. The dashed line in each plot shows the percolation transition curve as predicted by Eqs. 13 and 14. All other parameters are the same as in Fig. 2.

correspond to calculations involving the Lagarkov-Sarychev approach. We note from these graphics that for each value of L there exists an optimum filling factor f that maximises the decay rate (brightest regions in the plots). Interestingly, the position of the peak of the SE rate in Fig. 4 is perfectly described by the percolation curves given in Eqs. (13) and (14), as shown by the dashed lines in the plots. These results demonstrate the robustness of our findings against variations of the shape of the inclusions as well as changes in effective theory used to model the electric permittivity ε_e of the composite medium. We checked that these conclusions are valid for both parallel (Γ_{\parallel}) and perpendicular (Γ_{\perp}) configurations and apply for all distances $z \lesssim 10 \mu\text{m}$. We have also verified that our results are not qualitatively modified by changing the material that constitute the metal inclusions. Indeed, in Table I, we show the ratio between Γ_{\parallel} at the percolation threshold ($f = f_c$) and its value for a full metallic semi-infinite medium ($f = 1$) when the substrate is composed with different metal inclusions. In the table $L = 0.1$ corresponds to needle-like inclusions (eccentricity $e \simeq 0.95$) and $L = 1/3$ to spherical ones ($e = 0$). The enhancement in the SE rate Γ_{\parallel} is at least two orders of magnitude, regardless of the metal and the effective medium theory considered. We emphasize that the same effect occurs for the Γ_{\perp} rate. These results provide evidence that our findings should hold even beyond the effective medium approximation. The differences in the results obtained by means of the BEMT and the Lagarkov-Sarychev model for $L = 0.1$ are due to the distinct assumptions made about the host dielectric medium (see Sec. II B and Refs. [31–33, 35]).

	Bruggeman		Lagarkov-Sarychev	
	$L = 0.1$	$L = 1/3$	$L = 0.1$	$L = 1/3$
Au	794	524	116	524
Cu	1099	726	104	726
Ti	190	127	127	127
Ag	923	610	108	610

Table I. Values for the ratio $\Gamma_{\parallel}(f = f_c)/\Gamma_{\parallel}(f = 1)$ for different metallic inclusions. All values were computed by considering a Polystyrene host medium, an emitter-substrate distance of 50 nm, and emission wavelength of $450\mu\text{m}$.

We should mention that our results apply for a broad range of transition frequencies and could be tested using quantum emitters working from THz to near-infrared. In Fig. 5, the SE rate in the parallel configuration is calculated using BEMT as a function of both transition frequency ω and volume filling factor f considering spherical gold inclusions ($L = 1/3$) at $z = 50\text{ nm}$ distance between the emitter and the composite media. The maximum emission always takes place at the percolation threshold f_c^B . At larger frequencies the insulator-metal transition effect on the emitter's lifetime becomes weaker and a broadening of the emission peak occurs. This behavior is due to the fact that, for larger and larger frequencies, the distinction between dielectrics and conductors becomes less and less pronounced, thus making the percolation transition less dramatic. We have verified that similar results hold in the perpendicular configuration; they also apply within the Lagarkov-Sarychev model.

In Fig. 6, we investigate the role of the different decay channels in the SE rate. The decay probability of the quantum emission is shown in terms of propagating (Prop), totally internal reflected (TIR) or evanescent modes (Eva) as a function of the filling factor f and the distance z between the atom and the semi-infinite medium. The probabilities are computed as the ratio between the partial and the total SE rate. The partial contribution of these modes to decay rates can be expressed as [25]

$$\begin{aligned} \frac{\Gamma_{\perp}^{\text{Prop}}}{\Gamma^{(0)}}(z) &= 1 + \frac{3}{2} \int_0^{k_0} \frac{k_{\parallel}^3}{k_0^3 \zeta} \text{Re} [r^{\text{TM, TM}} e^{2i\zeta z}] dk_{\parallel} \\ \frac{\Gamma_{\perp}^{\text{TIR}}}{\Gamma^{(0)}}(z) &= \frac{3}{2} \int_{k_0}^{n_e k_0} \frac{k_{\parallel}^3}{k_0^3 \zeta} e^{-2\zeta z} \text{Im} [r^{\text{TM, TM}}] dk_{\parallel} \\ \frac{\Gamma_{\perp}^{\text{Eva}}}{\Gamma^{(0)}}(z) &= \frac{3}{2} \int_{n_e k_0}^{\infty} \frac{k_{\parallel}^3}{k_0^3 \zeta} e^{-2\zeta z} \text{Im} [r^{\text{TM, TM}}] dk_{\parallel}, \quad (20) \end{aligned}$$

where we defined the medium index of refraction $n_e = \text{Re}\sqrt{\varepsilon_e/\varepsilon_0}$. In Fig. 6(a) we see clearly that for $f \leq f_c$, the contribution of the evanescent modes quickly rises and dominates the decay process. Despite the fact that the medium behaves effectively as a dielectric in this regime, it is the dissipation in the metallic inclusions that actually gives rise to such a dominance. Once we step into the $f > f_c$ region, we see that evanescent and TIR modes progressively swap roles, and the latter becomes the most important decay channel. This happens because n_e grows steadily as a function of f in the metallic regime, so there are more TIR modes available as the filling

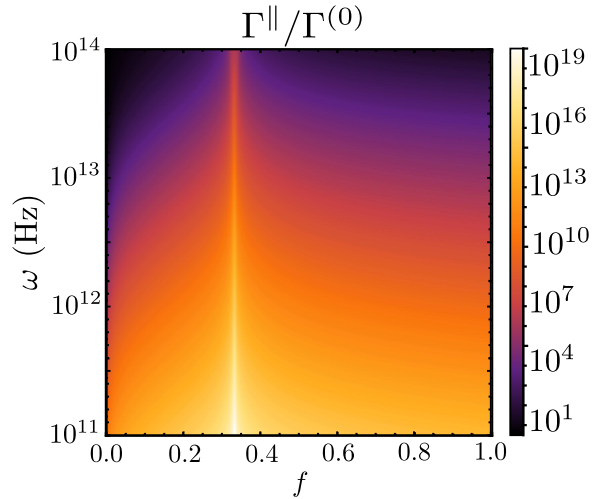


Figure 5. The two-dimensional plot displays the ratio $\Gamma_{\parallel}/\Gamma^{(0)}$ using the BEMT as a function of the filling factor f and the quantum emitter frequency ω . The enhancement of the SE rate reaches its maximum precisely at percolation transition $f = f_c^B = 1/3$ (for spherical inclusions). A similar behavior has been verified for the perpendicular case $\Gamma_{\perp}/\Gamma^{(0)}$.

factor is increased. In addition, in Fig. 6(b) we show the different decay pathways right at the percolation threshold [39], as a function of distance. For short distances, the enhancement in SE is due mainly to the evanescent contribution, meaning that the energy associated with the decay is (with very high probability) absorbed by the half-space [40]. As the distance increases, the contribution of evanescent modes decreases and propagating and TIR modes become more important.

In Fig. 7, the contribution to the SE rate due to evanescent modes is shown as a function of both f and z . It can be noted that, for $z \lesssim 100\text{ nm}$, the probability of decaying in an evanescent mode is larger than 60% (and even larger when the media behaves like dielectric $f < f_c^B$). We should also stress out that at the percolation $f = f_c^B = 1/3$ (for spherical inclusions) the contribution of evanescent modes are relevant even for larger distances of about $z \lesssim 1\mu\text{m}$.

IV. CONCLUSIONS

We have investigated the spontaneous emission rate of a two-level atom in the vicinities of a semi-infinite medium composed of randomly dispersed, arbitrary shaped gold inclusions embedded in a polystyrene host matrix. Using effective medium theories to describe the electromagnetic properties of the composite medium, we demonstrate that the presence of composite media is responsible for a great enhancement of the SE rate relative to the homogeneous semi-infinite medium case. We find that this enhancement in the SE rate is maximal at the percolation critical point for the composite medium, where it can be as impressive as two orders of magnitude. The enhancement in the spontaneous emission rate is more pronounced at small distances between the emitter and

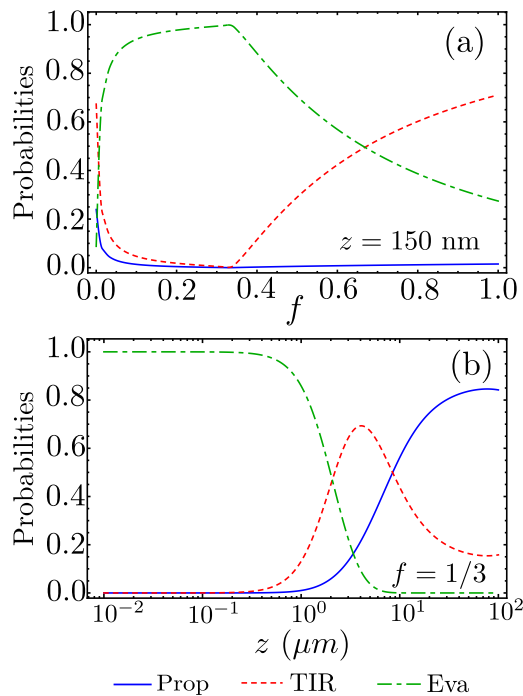


Figure 6. The decay channel probability of the quantum emission in the presence of the effective media (BEMT) with spherical inclusions ($L = 1/3$) is displayed as a function of both the filling factor f at a fixed distance $z = 150$ nm between the atom and the media (a) and as a function of z at the percolation threshold $f = 1/3$ (b).

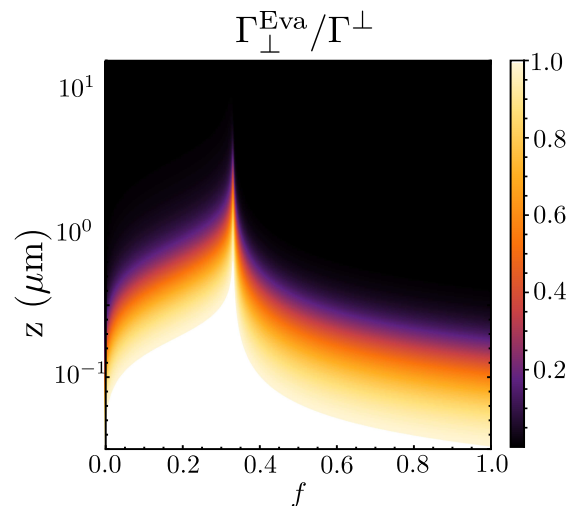


Figure 7. The quantum emission into evanescent modes is displayed as a function of both the distance between the emitter and the media z and the filling factor f .

the composite medium, unveiling the crucial role of near field effects. In addition, we show that our results are robust against material losses, to changes in the shape of inclusions and materials, for a broad range of transition frequency, and apply for different effective medium theories. We also investigate the contribution of different decaying channels in the SE rate. We hope that our findings could guide the design of composite media aiming at tailoring and optimizing the decay rate of quantum emitters.

ACKNOWLEDGEMENTS

We thank E. C. Marino and M. Hippert for useful discussions. D.S., F.S.S.R. and C. F. acknowledge CAPES, CNPq, and FAPERJ for financing this research. W.K.-K. thanks LANL LDRD project for financial support. F.A.P. thanks the hospitality of the Optoelectronics Research Centre and Centre for Photonic Metamaterials, University of Southampton, where part of this work has been done, and CAPES for funding his visit. F. A. P. acknowledges the financial support of the Royal Society (U.K.) through a Newton Advanced Fellowship (ref: NA150208), CAPES (Grant No. BEX 1497/14-6) and CNPq (Grant No. 303286/2013-0).

[1] E. M. Purcell, Phys. Rev. **69**, 681 (1946).
 [2] K.H. Drexhage, H. Kuhn and F.P. Schäfer, Phys. Chem. **72**, 329 (1968).
 [3] L. Novotny, and B. Hecht, *Principles of Nano-Optics* (Cambridge Univ. Press, 2006).
 [4] K. Joulain, R. Carminati, J-P.Mulet, and Greffet, Phys. Rev. B **68**, 245405 (2003).
 [5] E. Betzig, R. J. Chichester, Science **262**, 5138 (1993).

[6] R. X. Bian, R. C. Dunn, X. S. Dunn, and P. T. Leung, Phys. Rev. Lett. **75**, 4772 (1995).
 [7] E. J. Sanchez, L. Novotny, and X S. Xie, Phys. Rev. Lett. **82**, 4014 (1999).
 [8] J. B. Jackson and N. J. Halas, Proc. Natl. Acad. Sci. USA **101**, 17930 (2004).
 [9] H. Wei, F. Hao, Y. Huang, W. Wang, P. Nordlander, and H. Xu, Nano Lett. **8**, 2497 (2008).

- [10] J. F. Li, Y. F. Huang, Y. Ding, Z. L. Yang, S. B. Li, X. S. Zhou, F. R. Fan, W. Zhang, Z. Y. Zhou, D. Y. Wu, B. Ren, Z. L. Wang and Z. Q. Tian, *Nature (London)* **464**, 392 (2010).
- [11] Y. V. Vladimirova, V. V. Klimov, V. M. Pastukhov, and V. N. Zadkov, *Phys. Rev. A* **85** 053408 (2012).
- [12] P. Lodahl, A. F. van Driel, I. S. Nikolaev, A. Irman, K. Overgaag, D. Vanmaekelbergh and W. L. Vos, *Nature* **430**, 654 (2004).
- [13] J. M. Raimond, M. Brune, S. Haroche, *Rev. Mod. Phys.* **73**, 565 (2001).
- [14] L. Novotny and N. F. Hulst, *Nature Photon.* **5**, 83 (2011).
- [15] G. M. Akselrod, C. Argyropoulos, T. B. Hoang, C. Ciraci, C. Fang, J. Huang, D. R. Smith, and M. H. Mikkelsen, *Nature Photon.* **8**, 835 (2014).
- [16] W. J. M. Kort-Kamp, F. S. S. Rosa, F. A. Pinheiro, and C. Farina, *Phys. Rev. A* **87**, 023837 (2013).
- [17] W. J. M. Kort-Kamp, F. S. S. Rosa, F. A. Pinheiro, and C. Farina, *JOSA A* **31** (9), 1969 (2014).
- [18] C. L. Cortes, W. Newman, S. Molesky, and Z. Jacob, *J. Opt.* **14**, 063001 (2012).
- [19] A. V. Chebykin, A. A. Orlov, A. S. Shalin, A. N. Poddubny and P. A. Belov, *Phys. Rev. B* **91**, 205126 (2015).
- [20] D. A. Powell, A. Alù, B. Edwards, A. Vakil, Y. S. Kivshar, and N. Engheta, *Phys. Rev. B* **79**, 245135 (2009).
- [21] P. Ginzburg, F. J. Rodríguez Fortuño, G. A. Wurtz, W. Dickson, A. Murphy, F. Morgan, R. J. Pollard, I. Iorsh, A. Atrashchenko, P. A. Belov, Y. S. Kivshar, A. Nevet, G. Ankonina, M. Orenstein and A. V. Zayats, *Opt. Express* **21**, 14907 (2013).
- [22] R. Sokhoyan and H. A. Atwat, *Opt. Express* **21**, 32279 (2013).
- [23] V. V. Klimov, *Opt. Commun.* **211**, 183 (2002).
- [24] K. J. Tielrooij *et al.*, *Nature Physics* **11**, 281 (2015).
- [25] W. J. M. Kort-Kamp, B. Amorim, G. Bastos, F. A. Pinheiro, F. S. S. Rosa, N. M. R. Peres and C. Farina, *Phys. Rev. B* **92**, 205415 (2015).
- [26] V. Krachmalnicoff, E. Castanié, Y. De Wilde, and R. Carminati, *Phys. Rev. Lett.* **105**, 183901 (2010).
- [27] R. Sapienza, P. Bondareff, R. Pierrat, B. Habert, R. Carminati, and N. F. Van Hulst, *Phys. Rev. Lett.* **106**, 163902 (2011).
- [28] T. Nakamura, B. P. Tiwari, and S. Adachi, *Opt. Express* **20** 26548 (2012).
- [29] T. C. Choy, *Effective Medium Theory: Principles and Applications* (Oxford University Press, 1999).
- [30] A.N. Lagarkov and A.K. Sarychev, *Phys. Rev. B* **53** 6318 (1996).
- [31] F. Brouers, *J. Phys. C: Solid State Phys.* **19**, 7183 (1986).
- [32] A. V. Goncharenko and E. F. Venger, *Phys. Rev. E* **70** 057102 (2004).
- [33] M. Sahimi, *Applications of Percolation Theory* (Taylor and Francis, 1993), pp. 59.
- [34] W. J. M. Kort-Kamp, P. I. Caneda, F. S. S. Rosa, and F. A. Pinheiro, *Phys. Rev. B* **90**, 140202(R) (2014).
- [35] A.K. Sarychev and V. M. Shalaev, *Physics Reports*, **335** 275 (2000).
- [36] M. A. Ordal, Robert J. Bell, R. W. Alexander, Jr, L. L. Long, and M. R. Querry, *App. Opt.* **24**, 4493 (1985).
- [37] D. B. Hough, and L. R. White, *Adv. Coll. Int. Sci.* **14**, 3 (1980).
- [38] In Ref. [32], $\Gamma_1 = \Gamma_2 = 0$. Here, however, we decided to include small ohmic losses so as to make the model more realistic.
- [39] The percolation transition is defined in the limit $\omega \rightarrow 0$, and we, strictly speaking, are working at a finite frequency ($\omega_0 \approx 0.8$ THz). That makes critical filling factor $f_c = 1/3$ to be slightly off (we have actually $f_c \approx 0.336$), but this has absolutely no effect in our results.
- [40] G. W. Ford, and W. H. Weber, *Phys. Rep.* **113**, 195 (1985).